



Published in final edited form as:

Biomaterials. 2016 October ; 105: 25–37. doi:10.1016/j.biomaterials.2016.07.034.

Valve interstitial cell tensional homeostasis directs calcification and extracellular matrix remodeling processes via RhoA signaling

Emily J. Farrar^{1,3}, Varsha Pramit², Jennifer M. Richards³, Christopher Z. Mosher⁴, and Jonathan T. Butcher³

¹Department of Engineering, Messiah College, Mechanicsburg, PA

²Department of Chemical and Biomolecular Engineering, Cornell University, Ithaca NY

³School of Biomedical Engineering, Cornell University, Ithaca, NY

⁴Department of Biomedical Engineering, Case Western Reserve University, Cleveland OH

Abstract

Aims—Valve interstitial cells are active and aggressive players in aortic valve calcification, but their dynamic mediation of mechanically-induced calcific remodeling is not well understood. The goal of this study was to elucidate the feedback loop between valve interstitial cell and calcification mechanics using a novel three-dimensional culture system that allows investigation of the active interplay between cells, disease, and the mechanical valve environment.

Methods & Results—We designed and characterized a novel bioreactor system for quantifying aortic valve interstitial cell contractility in 3-D hydrogels in control and osteogenic conditions over 14 days. Interstitial cells demonstrated a marked ability to exert contractile force on their environment and to align collagen fibers with the direction of tension. Osteogenic environment disrupted interstitial cell contractility and led to disorganization of the collagen matrix, concurrent with increased α SMA, TGF- β , Runx2 and calcific nodule formation. Interestingly, RhoA was also increased in osteogenic condition, pointing to an aberrant hyperactivation of valve interstitial cells mechanical activity in disease. This was confirmed by inhibition of RhoA experiments. Inhibition of RhoA concurrent with osteogenic treatment reduced pro-osteogenic signaling and calcific nodule formation. Time-course correlation analysis indicated a significant correlation between interstitial cell remodeling of collagen fibers and calcification events.

Conclusions—Interstitial cell contractility mediates internal stress state and organization of the aortic valve extracellular matrix. Osteogenesis disrupts interstitial cell mechanical phenotype and drives disorganization, nodule formation, and pro-calcific signaling via a RhoA-dependent mechanism.

Address for correspondence: Jonathan T. Butcher, PhD, Associate Professor, Associate Director, Director of Undergraduate Studies, Nancy E. and Peter C. Meinig School of Biomedical Engineering, 304 Weill Hall, Cornell University, Ithaca, NY 14853-7202, Phone: 607-255-3575, Fax: 607-255-7330, jtb47@cornell.edu.

Publisher's Disclaimer: This is a PDF file of an unedited manuscript that has been accepted for publication. As a service to our customers we are providing this early version of the manuscript. The manuscript will undergo copyediting, typesetting, and review of the resulting proof before it is published in its final citable form. Please note that during the production process errors may be discovered which could affect the content, and all legal disclaimers that apply to the journal pertain.

Keywords

Stress fiber; f-actin; compaction; bioreactor; alpha-smooth muscle actin; alignment; SOX9; MMP-9; mechanobiology; biomechanics; myofibroblast; activation

Introduction

Aortic valve disease (AVD) is a leading cause of cardiovascular morbidity resulting in approximately 15,000 deaths per year in the USA. It is primarily a disease of the elderly, occurring in 2.8% of Americans over the age of 75 [1]. It is an active degenerative process driven by complex cell-cell and cell-matrix interactions [2]. Despite sharing risk factors with atherosclerosis [3], it is a pathobiologically unique disease that has no clinically proven biologically-based intervention strategies outside of cardiothoracic surgery [4].

As the aortic valve becomes diseased, its mechanics change in a number of ways. The leaflets stiffen as calcific nodules form [5], the extracellular matrix becomes disorganized [6] and altered in composition [7], and the strain experienced by valvular interstitial cells (VIC) increases [8]. These changes influence VIC phenotype and modulate VIC interactions with their environs [9, 10]. Strain state regulates VIC cytokine secretion [11,12], calcification [13], collagen synthesis [14], alignment [15], and proliferation [16]. Extracellular matrix composition influences VIC homeostasis [17], in part through modulation of leaflet [18] and cellular [19] stiffness. VIC become activated in response to changes in their mechanical [20] or biochemical [21] situation, initiating a complex feedback loop between cellular decisions and changes in the extracellular environment. The temporal dynamics of this loop, as well as the role of disease progression on signaling, are not well understood. Understanding the time and phase governance of the mechanical-biological interplay in AVD is critical to the design of effective interventions that could capitalize on biological signaling cascades, rather than drug- or surgical-based strategies.

In this study, we have designed a novel system to culture VIC in 3D hydrogels with a controlled and sustained level of tension. The system allows measurement of dynamic tissue stresses developing within a 3D VIC and collagen environment, as well as imaging of changes to collagen and cell morphology via longitudinal confocal microscopy. This system allowed us to uniquely investigate the interplay between collagen fibers, cell morphology, activity, and signaling, and osteogenesis in order to shed light on the complex mechanopathology of aortic valve disease. We identified a distinct tri-phasic temporal mechanobiological response of VIC to osteogenic environment. We further show that the tri-phasic remodeling and mechanobiological response is disrupted by RhoA inhibition.

Materials and Methods

Bioreactor System Fabrication

The systems were created using a custom mold, polydimethylsiloxane (PDMS) at a 15:1 base to curing agent ratio, and steel springs. A collagen hydrogel seeded with porcine aortic valve interstitial cells (PAVIC) was pipetted into the system with the use of a PDMS plug to help the hydrogel stay in place. The plug was then removed in 30 minutes, after the hydrogel

had set (Fig. 1). PAVIC used in the system were harvested from fresh porcine aortic valves from a local abattoir, cultured up to a maximum of six passages, and seeded at 1 million cells per milliliter into a 1 mg/mL type I collagen hydrogel (rat-tail collagen, Corning, 354236), as described previously [15]. Hydrogel in the spring system were cultured in either control medium or osteogenic medium. Control medium was made from Dulbecco's Modified Eagle Medium (ThermoFisher Scientific Scientific, 12100061) with 10% fetal bovine serum (ThermoFisher Scientific Scientific, 10437028) and 1% penicillin-streptomycin (ThermoFisher Scientific Scientific, 15140122). Osteogenic medium was made from control media supplemented with 10 mMol/L β -glycerophosphate (Sigma, G9422), sterile filtered 50 mg/mL ascorbic acid (Sigma, 1043003 USP), and 10 nMol/L dexamethasone (Sigma, D4902) for 14 days with media changed every 48 hours.

Effect of varying spring parameters

Two different springs (Table 1) were tested for their ability to recapitulate physiological tissue stress levels in the hydrogels over 14 days of culture. Both springs were made of SS316 stainless steel and obtained from Lee Spring Company.

Each spring was cut to nine centimeter length and inserted into the system. The load required to cause deflection of the end of the springs between zero and one millimeter was measured for each spring system by downward translation of the spring onto a high-precision scale (Fig. 2A, B). This process was repeated using five different systems for each type of spring, with all five springs obtained from the same batch from Lee Spring Company, to estimate variation between springs. A cantilevered beam approximation was used to calculate the effective modulus (EI) of each type of spring according to equation 1.

$$\delta_{max} = \frac{PL^3}{3EI} \quad (1)$$

Imaging Gels

To measure spring deflection, the systems were live-imaged in a sterile environment using an inverted dissection microscope with a Lumenera INFINITY 1-5 5.0 megapixel CMOS digital camera at 0.67 \times magnification. Deflection of the spring was measured with ImageJ and used to calculate contractile force according to the calculated effective modulus for each spring. The thickness of each gel was also measured at the thinnest point at the middle of each gel. Using the center of the gel ensured that results were not affected by boundary conditions caused by the interaction of the spring and the hydrogel, which were quantified using confocal microscopy of collagen and cell fiber orientation (as described below) and found to extend only 1 millimeter from the spring into the hydrogel. The gels were assumed to be perfectly cylindrical at the center, thus the area was calculated from equation 2.

$$\text{Area}_{gel} = \pi * \text{thickness}^2 \quad (2)$$

Force and gel thickness were used to calculate contractile stress (σ) in the gel at the thinnest point, using equation 3.

$$\sigma = \frac{F_{VIC}}{Area_{gel}} \quad (3)$$

The internal stresses developed in each of the two types of spring systems were then compared over the course of the experiment (Fig. 2C). The two spring systems showed similar trends in stress in the hydrogels over time. However, the 0.008 inch wire diameter springs developed a significantly broader range of stresses over the 14 days (0-30 kPa versus 0-20 kPa) that were more representative of the stresses found in a human aortic valve *in vivo* [28], thus we selected these springs for use in all following experiments.

VIC Phenotype

After 1, 5, or 14 days, VIC RNA was isolated harvested from gels with the Qiagen RNeasy kit (Qiagen, 74104) according to the manufacturer's instructions. cDNA was synthesized using the iScript cDNA synthesis kit (Bio-Rad, 170-8891), according to the manufacturer's instructions using 20 nanograms of RNA template. Quantitative real-time PCR was performed using SYBR Green FastMix (Quanta, 95072-05K) as previously described [22] using the primers in Table 2.

Immunofluorescence, collagen imaging, and cell viability/cytotoxicity

Antibody and cytoskeletal staining was performed as described previously [22] using α SMA goat anti-rabbit (1:100, Abcam, ab5694), Alexa Fluor 488 Phalloidin (1:500, ThermoFisher Scientific, A12379), and DRAQ5 (1:1000, Cell Signaling Technologies, 4084) to detect alpha-smooth muscle actin, f-actin, and nuclei, respectively. Goat anti-rabbit Alexa Fluor 568 was used as a secondary antibody at 1:200 (ThermoFisher Scientific, AF-11011). Gels were imaged using a Zeiss 710 or 780 laser scanning confocal microscope. Collagen reflectance microscopy was used to simultaneously collect collagen fiber images.

Cell viability was assessed every 48 hours using the live/dead viability/cytotoxicity Kit for mammalian cells from ThermoFisher Scientific (L3224), according to the manufacturer's instructions and as described previously [23]. Briefly, the assay was performed by rinsing the intact hydrogel system in phosphate buffered saline (PBS, Sigma, P5493), incubating it fully submerged the staining solution for 30 minutes at room temperature, rinsing again in PBS, then imaging immediately using a Zeiss 710 laser scanning confocal microscope at 40 \times magnification. Immediately after imaging, fresh media was applied to the gels and the system was placed back at 37 $^{\circ}$ C. No system was out of incubation for more than ten minutes at any given time. The live/dead images were analyzed using ImageJ (NIH) to calculate the average number of live cells within three different viewing areas of the gel. This procedure was repeated on a single system seven different times, at days 1, 3, 5, 7, 9, 11 and 14. The full time-course of live/dead assays was repeated across four different systems.

Inhibition of RhoA was achieved using X-treme Gene 9 transfection reagent (Sigma, XTG9-RO ROCHE) according to the manufacturer's instructions, using 1 $\mu\text{g}/100 \mu\text{L}$ of dominant negative RhoA plasmid (gift from: Dr. Sanjay Kumar, Department of Bioengineering, University of California, Berkeley). The cells were used 24 hours after initial transfection.

Cell and collagen fiber alignment analysis

Interstitial cell f-actin fiber and collagen fibril alignment angle distributions were analyzed as previously described [15, 24]. Briefly, z-stack images of gels were collected via confocal and collagen reflectance microscopy, at a resolution of 2 μm per slice, for at least 200 μm of the total depth of the gel and up to 400 μm . Maximum intensity projections of 20 μm stacks for cells and fibers at the central region of each gel were compiled using ImageJ. The average of three representative 20 μm stacks was used to calculate alignment for each gel. Regions of distinct nodule formation in osteogenic condition were avoided, unless otherwise noted in text. F-actin and collagen fiber alignment was quantified using a MATLAB algorithm adapted from [24] and [15]. The algorithm uses a fast fourier transform to quantify the orientation of lines in an image. Briefly, the algorithm sums the FFT intensity along lines at increments of 5° from 0 to 180°, with 0° and 180° being fully aligned with the direction of tension in the hydrogel. The intensity that falls along lines at 0° and 180° is summed and divided by the total measured intensity to give a fiber alignment ratio. Therefore, a fiber alignment ratio of 1 indicates that 100% of the fibers in the image fall along lines of 0° or 180°. A fiber alignment of 0.4 indicates that 40% of the fibers in the image fall along lines of 0° or 180°. Given the complexity of the collagen structures and the use of z-stack projections to capture more of the hydrogel thickness, a fiber alignment ratio of 0.4 can be considered highly aligned with the direction of tension.

Statistics

Data is expressed as mean \pm standard error of the mean (SEM). All comparisons between two groups were made using two-tailed, unpaired t-tests assuming unequal variance. Comparisons between multiple groups were made using ANOVA with Tukey post hoc paired tests. Differences between means were considered significant when $p < 0.05$. Correlation analysis was done by finding Pearson's linear correlation coefficient between each set of variables. The significance of correlation was tested using a two-way Student's t-test. A correlation was considered statistically significant when $p < 0.05$.

Results

Design of system to culture VIC in 3D while measuring contractile force

The VIC seeded in the hydrogels within the system were well spread and quiescent (no αSMA) (Fig. 3A). Live/dead analysis indicated good viability over 14 days, with only a slight decrease to 94% live cells at day 7 in osteogenic gels and to 89% and 88% live cells at day 14 in control and osteogenic conditions, respectively (Fig. 3B). Cell density was consistent over 14 days, with a slight increase in control condition at day 7 and 14 due to compaction of the hydrogel (Fig. 3C).

Pro-osteogenic stimulation dysregulates the native ability of VIC to organize and maintain their mechanical environment

VIC in control condition were classified as normal VIC and VIC in osteogenic condition were classified as osteoblast-like VIC, due to their ability to deposit calcium and form nodules. We observed normal VIC and osteoblast-like VIC hydrogels in the bioreactor over 14 days and identified three phenotypic phases: acute (day 1), transitional (days 3-5), and advanced pathological (days 7-14). These phases are marked by changes in VIC RNA, protein, and mechanobiological activity, characterized by VIC influence on the collagen fibers of the hydrogel.

In the acute phase, stress, fiber alignment, and fiber density are higher in the osteoblast-like VIC gels than in controls. In the transition phase (days 3-5), stress, fiber alignment, and fiber density are equal in osteoblast-like VIC and controls. Osteoblast-like VIC and control gels are also thinning at approximately the same rate during the transition phase. In the advanced pathological phase, osteoblast-like VIC gels are significantly thicker and have significantly lower stress, density, and fiber alignment (Fig. 4).

Therefore, we found that VIC in our system show three distinct phases of mechanobiological response to pro-osteogenic stimulation. In the acute phase, osteoblast-like VIC are more active than normal VIC, the hydrogel is under more internal stress, and the fibers are more aligned and dense. In the transition phase, osteoblast-like VIC and normal VIC activity appears equal, as the hydrogels show equal internal stress, fiber alignment, and density. In the advanced pathological phase, osteoblast-like VIC show a signature mechanobiological response, in which the gels are thicker, lower stress, less aligned, and have less dense collagen than normal VIC.

Dysregulation of VIC morphology and myofibroblastic signaling correlates with phases of mechano-osteogenic response

We assessed cell morphology, f-actin fiber dynamics, and α SMA expression at each phase of VIC response. We found that normal VIC have consistent alignment of cell cytoskeleton with direction of tension and only slight increase in α SMA over 14 days. In contrast, osteoblast-like VIC have f-actin fibers aligned with the direction of tension at day 1, but increasing disorganization and expression of α SMA at day 5 and even more so at day 14 (Fig. 5A). Quantification of f-actin fiber directionality showed decreasing alignment of osteoblast-like VIC cytoskeleton over time relative to normal VIC (Fig. 5B). We then analyzed mRNA levels of mechanotransductive protein RhoA and myofibroblastic marker α SMA (ACTA2 gene) at each phase of response. Osteoblast-like VIC had higher levels of RhoA mRNA than normal VIC at day 1, indicating an aggressive initial mechanotransductive response. RhoA mRNA decreased over time in both osteoblast-like VIC and normal VIC. α SMA increased similarly over the first two phases (day 1 and 5) in both normal VIC and osteoblast-like VIC. However, at the third phase (day 14), osteoblast-like VIC had significantly higher expression of α SMA (Fig. 5C).

Pro-osteogenic environment disrupts ability of VIC to organize collagen matrix

Collagen fiber imaging revealed significant changes in the collagen hydrogel environment at each phase of VIC response to osteogenic. In the acute phase (day 1), osteoblast-like VIC drove increased alignment of collagen fibers in the direction of gel tension compared to normal VIC. In the transition phase (day 5), fiber alignment is similar in both normal VIC and osteoblast-like VIC gels. However, as VIC reached the advanced pathological phase (day 14), normal VIC gels had fiber alignment similar to day 5, but osteoblast-like VIC gel fibers are highly disorganized (Fig. 6A).

Analysis of collagen isoform mRNA showed a corresponding switch from the acute to the transition phase, with exaggerated response at the advanced phase. Specifically, Collagen I was lower in osteoblast-like VIC at day 1, but increased over time and was higher than nVIC at all later stages. Normal VIC synthesized increasing amounts of collagen II over time, whereas osteoblast-like VIC plateaued in their level of collagen II mRNA synthesis across days 1-14. Collagen III was similar in normal VIC and osteoblast-like VIC at day 1, but was significantly higher in osteoblast-like VIC from day 5 onwards (Fig. 6B).

We then examined MMP-9 mRNA for an indication of matrix remodeling activity and Sox-9 as a marker of chondrogenic differentiation. In the acute phase, MMP-9 was lower in osteoblast-like VIC, but in the transition phase osteoblast-like VIC had significantly higher MMP-9 than nVIC. Both normal VIC and osteoblast-like VIC had almost undetectable MMP-9 mRNA at the advanced phase. Sox9, a transcriptional driver of chondrogenic differentiation that is regulated by RhoA and repressed in calcifying valves, was repressed in osteoblast-like VIC at the transition and advanced phases compared to normal VIC. Normal VIC showed increased Sox9 mRNA at the advanced phase compared to earlier phases (Fig. 6C).

Early increase in TGF- β 1 drives progressive pro-calcific phenotype of osteogenic VIC gels

Low-magnification bright field images revealed increasing nodule formation in osteoblast-like VIC gels over time (Fig. 7A, arrows). Confocal microscopy of nodules at the transition (day 5) and advanced (day 14) phases showed that nodules consisted of cell aggregates positive for α SMA (Fig 7B), cell aggregation, and significant disruption of collagen architecture near nodules. Quantification of nodules over time indicated significantly higher nodule formation in osteoblast-like VIC gels versus normal VIC at transition and advanced phases (Fig. 7C). Pro-calcific cytokine TGF- β 1 was increased in osteoblast-like VIC compared to normal VIC at the initial phase, but not at transition or advanced phases (Fig. 7D). Pro-osteogenic transcription factor Runx2 was higher in osteoblast-like VIC at all time points. ALP mRNA was the most drastically increased pro-osteogenic signaling factor we observed in osteoblast-like VIC, reaching over 1000-fold versus normal VIC the by the transition phase time point and maintaining highly upregulated levels through the advanced phase.

Inhibition of RhoA suppresses osteogenic and promotes chondrogenic VIC phenotype

In order to investigate the role of RhoA in VIC osteogenic response over time, we transfected VIC with a dominant-negative form of RhoA prior to seeding in the hydrogels

within the spring system. We found that DN-RhoA significantly decreased the number of nodules formed by VIC in the osteogenic environment, compared to VIC transfected with a control vector (Fig. 8A, B). This was not due to an increase in apoptosis. Over 90% of cells were viable at day 14 in both control and osteogenic conditions, in both empty vector and +DN-RhoA VIC (Fig. 8 C, D). In the advanced phase, DN-RhoA decreased fiber alignment and density in both control and osteogenic conditions compared to empty vector controls (Fig. 8E, F). DN-RhoA also led to increased gel thickness in both control and osteogenic conditions (Fig. 8G).

We then examined cellular mRNA signaling profiles in VIC+DN-RhoA at the advanced pathological phase (Fig. 8H). ACTA2 levels were the same, but MMP-9 increases were blocked by DN-RhoA transfection. Sox9 transcription was highly increased in the osteogenic condition. Collagen I and III mRNA were significantly decreased and collagen II was increased in DN-RhoA compared to controls. Pro-calcific signaling genes ALP, TGF- β 1, and Runx2 were uniformly downregulated in VIC+DN-RhoA, in both control and osteogenic environments.

Collagen fiber dynamics correlate with VIC mechanobiological activity

We then analyzed the mechanical and pathological changes in VIC systems over time to assess correlations between different variables. In normal VIC gels, collagen fiber density increased as fiber alignment increased ($p=0.03$). This correlation was lost in osteoblast-like VIC gels ($p=0.14$) (Fig. 9A). In nVIC gels, gel thickness decreased as fiber alignment increased ($p=0.05$). Loss of organized collagen structure and nodule formation degraded this correlation in osteoblast-like VIC gels ($p=0.14$) (Fig. 9B).

In normal VIC gels, gel thickness decreased as fiber density increased ($p=1.6E-5$). In osteoblast-like VIC gels, gels did not undergo thinning as density increased because of the increasing disorganization of collagen fibers over time ($p=0.16$) (Fig. 9C). In normal VIC gels, internal stress increased as fiber density increased ($p=0.01$). In osteoblast-like VIC gels, relationship between stress and density was not as strong due to loss of collagen organization and nodule formation ($p=0.22$) (Fig. 9D).

In osteoblast-like VIC gels, there was increased nodule formation as collagen fiber alignment decreased and thickness of the gels decreased ($p=0.01$, $p=0.02$ respectively). Normal VIC gels did not show any trends with respect to nodule formation, as there were no observable nodules (Fig. 9E, F).

Discussion

Importance of our novel system design

Our system is inexpensive, easily manufactured, and amenable to a variety of sterilization techniques including autoclaving. As shown here, the system can be live-imaged without disassembly allowing for dynamic longitudinal studies, which is an advantage over methods that require fixation and sectioning of the hydrogel prior to imaging [25]. Multiple types of springs can be used in the system to achieve a range of resulting internal stresses. Our system is designed to measure tissue-level stress, which adds to current knowledge of cell-

level mechanobiology [27]. In this study, the system is used specifically to replicate the healthy valve environment with a physiological cell number and density using collagen as our primary extracellular matrix component. This is useful for understanding native aortic valve biomechanics and how they progress from health to disease, in contrast to studies that focus on the damaged or diseased valve environment by using fibrin-based hydrogels [28]. Finally, the ability to tune the hydrogel matrix and its cellular components complements existing studies that use *ex vivo* valve tissue [29], allowing for a controlled investigation of the contribution of different physiological elements.

Identification of acute, transition, and advanced phases of VIC mechano-pathological response

Previous studies examining the dynamics of VIC mechanics in valve pathology have been conducted over very short time periods (less than 72 hours) [7,14,16,17,29]. However, degeneration of the aortic valve occurs over much longer time scales *in vivo*, and *in vitro* calcification has been shown in some studies to take at least 14 days to develop [31]. Studies that have examined longer time periods, 21 days [26] and 14 days [32], have only focused on the end time point. This study presents 14-day data and also reveals important intermediate phases (day 1 and day 5) that have not been shown previously (Fig. 10). We found that at day one, osteoblast-like VIC exert more stress, have higher fiber alignment, and higher fiber density. We characterize this as the acute phase of VIC mechanoreactive response to the osteogenic, pathological environment. Interestingly, by day five, we observed that normal VIC and osteoblast-like VIC exert similar stress and have similar fiber alignment and density. We characterize this as the transition phase in which osteoblast-like VIC have begun aggregate into nodule-like formations, have increased osteogenic signaling, and significant disruption of cell alignment, but have not yet significantly remodeled their collagen environment. Finally, at day 14, we saw advanced cell aggregate formation and pro-calcific signaling and significant changes in collagen fiber alignment and density. We characterize this as the advanced pathological phase of VIC mechanopathological response.

TGF- β 1 is an important mediator of VIC mechanopathology in the acute phase

TGF- β 1 increase is likely connected to the increase in RhoA in the acute phase (day 1), increasing cell tension and prompting the early contractile response of VIC to osteogenic media, as has been shown in fibroblasts [33]. Early TGF- β 1 activity also underpins the observed pro-fibrotic response of VIC [34], increased collagen synthesis [35], and the beginnings of the calcification response [36] (Fig. 11).

Many VIC calcification studies supplement osteogenic media with TGF- β 1 [31], despite TGF- β 1 being an important autocrine and paracrine signal that develops throughout valve calcification [37]. In this study, TGF- β 1 is not added to the osteogenic media, allowing VIC to produce their own TGF- β 1 at the acute phase. Our longitudinal results indicate that TGF- β 1 is an important early responder to osteogenic conditions. This agrees with studies in osteoprecursor cells that indicate that endogenous TGF- β 1 production is increased by both ascorbic acid and β -glycerophosphate [38], components of our osteogenic media. TGF- β 1 also induces rapid ALP expression in osteoblastic differentiation [39] and targets Runx2 transcriptional activity [40].

Changes in collagen organization dominate the transition phase

A recent study showed that collagen disruption or deficiency is sufficient to induce calcification in aortic valve leaflets [18]. Our results showed increased organization and elevated density of collagen osteogenic media condition in the acute phase, but this trend had leveled out by the transition phase (day 5) and was reversed by the advanced phase (day 14). This suggests that VIC induce an early, pro-fibrotic increase in collagen in response to osteogenic stimuli that changes to a pro-calcific decrease in collagen synthesis [41] through the transition (day 5) and advanced pathological (day 14) phases. Our mRNA results indicate that this phenomenon is dominated by changes in collagen II synthesis, which is lower than control at both day 5 and day 14, as opposed to collagen I or III.

Tension promotes early and aggressive calcification, dependent on RhoA activity

Both Runx2 and ALP are upregulated in the acute phase of osteogenic media stimulation (day 1). Dominant response then switches to ALP in the transition phase (day 5). By the advanced phase (day 14), both factors are again in effect. This early and sustained pro-osteogenic cell signaling demonstrates the importance of a physiologically-relevant tensioned environment in stimulating VIC response to pro-calcific stimuli. Osteogenic media also inhibited the increases in internal stress over time seen in normal VIC, indicating a change in the ability of osteoblast-like VIC to regulate valve leaflet stiffness [30] and respond to vasoactive agents [32].

The aggressive early mechanopathological calcification response is likely mediated by TGF- β 1 via RhoA signaling, as suppression of RhoA activation via transfection with DN-RhoA decreased both fiber alignment and density, suppressing collagen I and III synthesis and increasing expression of collagen II. DN-RhoA also decreased expression of ALP and Runx2 and increased expression of Sox9, suggesting a switch from pro-calcific to pro-chondrogenic phenotype [42]. Inhibition of RhoA may also block the trafficking of molecules involved in VIC mineralization. For example, a recent study showed that mechanical strain promoted calcification by stimulating localization of ENPP1 to the cell membrane via RhoA/ROCK signaling [43]. Our results provide strong evidence that RhoA is a major regulator of the phenotype and mechanical activity of VIC under osteogenic stimuli.

Interestingly, our system showed that osteoblast-like VIC actively remodel their environment and compact the gel as a whole, but to a lesser overall extent than normal VIC. Although normal VIC gels are thinner than osteoblast-like VIC gels from day 11-14, osteoblast-like VIC nodule formation correlates with progressive thinning of the osteoblast-like VIC gels. This is likely due to the overall increased mechanical activity of osteoblast-like VIC over time, despite the disorganization of their mechanical response. Decreased collagen II synthesis and decreased fiber density also contribute to the thickness of osteoblast-like VIC gels in the advanced pathological phase. This indicates that these osteoblast-like VIC and normal VIC phenotypes, seen *in vivo* in calcified human aortic valves, can be explained as the same original cell type (VIC) that have taken on a different phenotypic state due to their mechanobiological feedback with their environment.

VIC actively regulate their mechanical environment to maintain tissue homeostasis –this role is disrupted by pathological osteogenic differentiation

Our results provide evidence for an active role of VIC in maintaining the collagen environment of a healthy valve via increasing collagen fiber alignment and density over time, continuing synthesis and regulation of collagen isoforms, and generation of contractile force. These activities are disrupted as VIC undergo pathological response to osteogenic stimulation. Osteogenic environment disrupted cell and collagen fiber alignment, inhibiting the ability of VIC to compact and organize their extracellular matrix environment as they would in healthy tissue.

Conclusions

This study affirms the importance of VIC regulation of the extracellular matrix (ECM) in both homeostasis and disease. The VIC-ECM feedback loop is actively involved in maintenance of the valve matrix, as well as the pathogenesis of CAVD through the modulation of biochemical and biomechanical signals [44]. ECM disruption also creates a negative feedback loop between cell and matrix mechanics, changes surface receptor binding, disrupts paracrine signaling, and changes transduction of force through the extracellular environment [17]. Analysis of collagen isoforms and MMP-9 mRNA indicated VIC ECM changes are mediated by both synthesis of new collagen and by reorganization of the existing matrix. In particular, in the acute phase, osteoblast-like VIC showed increased collagen II mRNA and decreased MMP-9, indicating that the initial ECM response is mediated primarily by new collagen synthesis and not by matrix reorganization. In the transition phase, collagen II was decreased and MMP-9 was increased, pointing to a shift from synthesis to reorganization of collagen fibers. This is an important feature of dynamic VIC-matrix interaction that agrees with previous observations of valve thickening and fibrosis [45] followed by matrix disorganization [46,47].

REFERENCES

1. Mozaffarian D, Benjamin EJ, Go AS, Arnett DK, et al. Heart Disease and Stroke Statistics - 2015 Update. *Circulation*. 2015; 131:e29–e322. [PubMed: 25520374]
2. Rajamannan NM, Evans FJ, Aikawa E, Grande-Allen KJ, Demer LL, et al. Calcific Aortic Valve Disease: Not Simply a Degenerative Process. *Circulation*. 2011; 124:1783–1791. [PubMed: 22007101]
3. Stewart BF, Siscovick D, Lind BK, Gardin JM, Gottdiener JS, et al. Clinical Factors Associated With Calcific Aortic Valve Disease. *Journal of the American College of Cardiology*. 1997; 29:630–634. [PubMed: 9060903]
4. Cawley PJ, Otto CM. Prevention of calcific aortic valve stenosis—fact or fiction? *Ann Med*. 2009; 41:100–108. [PubMed: 18720096]
5. Freeman RV, Otto CM. Spectrum of Calcific Aortic Valve Disease: Pathogenesis, Disease Progression, and Treatment Strategies. *Circulation*. 2005; 111:3316–3326. [PubMed: 15967862]
6. Latif N, Sarathchandra P, Taylor PM, Antoniw J, Yacoub MH. Localization and pattern of expression of extracellular matrix components in human heart valves. *The Journal of Heart Valve Disease*. 2005; 14:218–227. [PubMed: 15792183]
7. Chen JH, Simmons CA. Cell-Matrix Interactions in the Pathobiology of Calcific Aortic Valve Disease: Critical Roles for Matricellular, Matricrine, and Matrix Mechanics Cues. *Circulation Research*. 2011; 108:1510–1524. [PubMed: 21659654]

8. Butcher JT, Simmons CA, Warnock JN. Mechanobiology of the Aortic Heart Valve. *Journal of Heart Valve Disease*. 2007; 17:62–73. [PubMed: 18365571]
9. Taylor PM, Batten P, Brand NJ, Thomas PS, Yacoub MH. The cardiac valve interstitial cell. *The International Journal of Biochemistry & Cell Biology*. 2003; 35:113–118. [PubMed: 12479860]
10. Liu AC, Joag VR, Gotlieb AI. The Emerging Role of Valve Interstitial Cell Phenotypes in Regulating Heart Valve Pathobiology. *The American Journal of Pathology*. 2007; 171:1407–1418. [PubMed: 17823281]
11. Merryman WD, Lukoff HD, Long RA, Engelmayr GC Jr, Hopkins RA, et al. Synergistic effects of cyclic tension and transforming growth factor- β 1 on the aortic valve myofibroblast. *Cardiovascular Pathology*. 2007; 16:268–276. [PubMed: 17868877]
12. Walker GA, Masters KS, Shah DN, Anseth KS, Leinwand LA. Valvular myofibroblast activation by transforming growth factor-beta: implications for pathological extracellular matrix remodeling in heart valve disease. *Circulation Research*. 2004; 95:253–260. [PubMed: 15217906]
13. Fisher CI, Chen J, Merryman WD. Calcific nodule morphogenesis by heart valve interstitial cells is strain dependent. *Biomech Model Mechanobiol*. 2012; 12:5–17. [PubMed: 22307683]
14. Balachandran K, Bakay MA, Connolly JM, Zhang X, Yoganathan AP, et al. Aortic valve cyclic stretch causes increased remodeling activity and enhanced serotonin receptor responsiveness. *The Annals of Thoracic Surgery*. 2011; 92:147–153. [PubMed: 21718840]
15. Gould RA, Chin K, Santisakultarm TP, Dropkin A, Richards JM, et al. Cyclic strain anisotropy regulates valvular interstitial cell phenotype and tissue remodeling in three-dimensional culture. *Acta Biomaterialia*. 2012; 8:1710–1719. [PubMed: 22281945]
16. Balachandran K, Sucusky P, Jo H, Yoganathan AP. Elevated cyclic stretch alters matrix remodeling in aortic valve cusps: implications for degenerative aortic valve disease. *AJP: Heart and Circulatory Physiology*. 2009; 296:H756–H764. [PubMed: 19151254]
17. Li C, Xu S, Gotlieb AI. The progression of calcific aortic valve disease through injury, cell dysfunction, and disruptive biologic and physical force feedback loops. *Cardiovascular Pathology*. 2013; 22:1–8. [PubMed: 22795219]
18. Rodriguez KJ, Piechura LM, Porras AM, Masters KS. Manipulation of valve composition to elucidate the role of collagen in aortic valve calcification. *BMC Cardiovascular Disorders*. 2014; 14:1–10. [PubMed: 24400643]
19. Liu H, Sun Y, Simmons CA. Determination of local and global elastic moduli of valve interstitial cells cultured on soft substrates. *Journal of Biomechanics*. 2013; 46:1967–1971. [PubMed: 23746597]
20. Honda S, Miyamoto T, Watanabe T, Narumi T, Kadowaki S, et al. A novel mouse model of aortic valve stenosis induced by direct wire injury. *Arteriosclerosis, Thrombosis, & Vascular Biology*. 2014; 34:270–278.
21. Yu Z, Seya K, Daitoku K, Motomura S, Fukuda I, et al. Tumor necrosis factor- α accelerates the calcification of human aortic valve interstitial cells obtained from patients with calcific aortic valve stenosis via the BMP2-Dlx5 pathway. *Journal of Pharmacology and Experimental Therapeutics*. 2011; 337:16–23. [PubMed: 21205918]
22. Farrar EJ, Huntley GD, Butcher JT. Endothelial-derived oxidative stress drives myofibroblastic activation and calcification of the aortic valve. *PLoS One*. 2015; 10:e0123257. [PubMed: 25874717]
23. Y. Duan B, Hockaday LA, Kang KH, Butcher JT. 3D Bioprinting of Heterogeneous Aortic Valve Conduits with Alginate/Gelatin Hydrogels. *Journal of Biomedical Materials Research A*. 2013; 101:1255–1264.
24. Bowles RD, Williams RM, Zipfel WR, Bonassar LJ. Self-assembly of aligned tissue-engineered annulus fibrosus and intervertebral disc composite via collagen gel contraction. *Tissue Eng Part A*. 2010; 16:1339–1348. [PubMed: 19905878]
25. Serrao GW, Turnbull IC, Ancukiewicz D, Kim DE, Kao E, Cashman TJ, Hadri L, Hajjar RJ, Costa KD. Myocyte-depleted engineered cardiac tissues support therapeutic potential of mesenchymal stem cells. *Tissue Engineering Part A*. 2012; 18:1322–1333. [PubMed: 22500611]
26. Ferdous Z, Jo H, Nerem RM. Differences in valvular and vascular cell responses to strain in osteogenic media. *Biomaterials*. 2011; 32:2885–2893. [PubMed: 21284997]

27. Yang MT, Fu J, Wang Y-K, Desai RA, Chen CS. Assaying stem cell mechanobiology on microfabricated elastomeric substrates with geometrically modulated rigidity. *Nat Protoc.* 2011; 6:187–213. [PubMed: 21293460]
28. Kural MH, Billiar KL. Myofibroblast persistence with real-time changes in boundary stiffness. *Acta Biomaterialia.* 2016; 1:223–230. [PubMed: 26712600]
29. Kershaw JD, Misfeld M, Sievers HH, Yacoub MH, Chester AH. Specific regional and directional contractile responses of aortic cusp tissue. *Journal of Heart Valve Disease.* 2004; 13:798–803. [PubMed: 15473483]
30. David Merryman W, Shadow Huang H-Y, Schoen FJ, Sacks MS. The effects of cellular contraction on aortic valve leaflet flexural stiffness. *Journal of Biomechanics.* 2006; 39:88–96. [PubMed: 16271591]
31. Cloyd KL, El-Hamamsy I, Boonrungsiman S, Hedegaard M, Gentleman E, et al. Characterization of Porcine Aortic Valvular Interstitial Cell “Calcified” Nodules. *PLoS ONE.* 2012; 7:e48154. [PubMed: 23110195]
32. Balachandran K, Sucusky P, Jo H, Yoganathan AP. Elevated Cyclic Stretch Induces Aortic Valve Calcification in a Bone Morphogenetic Protein-Dependent Manner. *The American Journal of Pathology.* 2010; 177:49–57. [PubMed: 20489151]
33. Meyer-ter-Vehn T, Sieprath S, Katzenberger B, Gebhardt S, Grehn F, et al. Contractility as a Prerequisite for TGF- β -Induced Myofibroblast Transdifferentiation in Human Tenon Fibroblasts. *Investigative Ophthalmology & Visual Science.* 2006; 47:4895–4904. [PubMed: 17065504]
34. Leask A, Abraham DJ. TGF- β signaling and the fibrotic response. *The FASEB Journal.* 2004; 18:816–827. [PubMed: 15117886]
35. Syedain ZH, Tranquillo RT. TGF- β 1 diminishes collagen production during long-term cyclic stretching of engineered connective tissue Implication of decreased ERK signaling. *Journal of Biomechanics.* 2011; 44:848–855. [PubMed: 21251657]
36. Clark-Greuel JN, Connolly JM, Sorichillo E, Narula NR, Rapoport HS, et al. Transforming Growth Factor- β 1 Mechanisms in Aortic Valve Calcification: Increased Alkaline Phosphatase and Related Events. *The Annals of Thoracic Surgery.* 2007; 83:946–953. [PubMed: 17307438]
37. Jian B, Narula N, Li Q-Y, Mohler ER III, Levy RJ. Progression of aortic valve stenosis: TGF- β 1 is present in calcified aortic valve cusps and promotes aortic valve interstitial cell calcification via apoptosis. *The Annals of Thoracic Surgery.* 2003; 75:457–465. [PubMed: 12607654]
38. Park J-B. The Effects of Dexamethasone, Ascorbic Acid, and b-Glycerophosphate on Osteoblastic Differentiation by Regulating Estrogen Receptor and Osteopontin Expression. *Journal of Surgical Research.* 2012; 173:99–104. [PubMed: 21035140]
39. de Gorter DJ, van Dinther M, Korchynskiy O, Dijke ten P. Biphasic effects of transforming growth factor β on bone morphogenetic protein-induced osteoblast differentiation. *J Bone Miner Res.* 2011; 26:1178–1187. [PubMed: 21611961]
40. Lee K-S, Kim H-J, Li Q-L, Chi X-Z, Ueta C, et al. Runx2 is a common target of transforming growth factor β 1 and bone morphogenetic protein 2, and cooperation between Runx2 and Smad5 induces osteoblast-specific gene expression in the pluripotent mesenchymal precursor cell line C2C12. *Molecular and Cellular Biology.* 2000; 20:8783–8792. [PubMed: 11073979]
41. Acharya A, Hans CP, Koenig SN, Nichols HA, Galindo CL, et al. Inhibitory Role of Notch1 in Calcific Aortic Valve Disease. *PLoS ONE.* 2011; 6:e27743. [PubMed: 22110751]
42. Peacock JD, Levay AK, Gillaspie DB, Tao G, Lincoln J. Reduced Sox9 Function Promotes Heart Valve Calcification Phenotypes In Vivo. *Circulation Research.* 2010; 106:712–719. [PubMed: 20056916]
43. Bouchareb R, Boulanger M-C, Fournier D, Pibarot P, Messaddeq Y, et al. Mechanical strain induces the production of spheroid mineralized microparticles in the aortic valve through a RhoA/ROCK-dependent mechanism. *Journal of Molecular and Cellular Cardiology.* 2014; 67:49–59. [PubMed: 24368096]
44. Fondard O, Detaint D, Lung B, Choqueux C, Adle-Biassette H, et al. Extracellular matrix remodelling in human aortic valve disease: the role of matrix metalloproteinases and their tissue inhibitors. *European Heart Journal.* 2005; 26:1333–1341. [PubMed: 15827062]

45. Leopold JA. Cellular mechanisms of aortic valve calcification. *Circulation: Cardiovascular Interventions*. 2012; 5:605–614. [PubMed: 22896576]
46. Hinton RB, Lincoln J, Deutsch GH, Osinska H, Manning PB, et al. Extracellular matrix remodeling and organization in developing and diseased aortic valves. *Circulation Research*. 2006; 98:1431–1438. [PubMed: 16645142]
47. Yip CYY, Chen JH, Zhao R, Simmons CA. Calcification by valve interstitial cells is regulated by the stiffness of the extracellular matrix. *Arteriosclerosis, Thrombosis, & Vascular Biology*. 2009; 29:936–942.

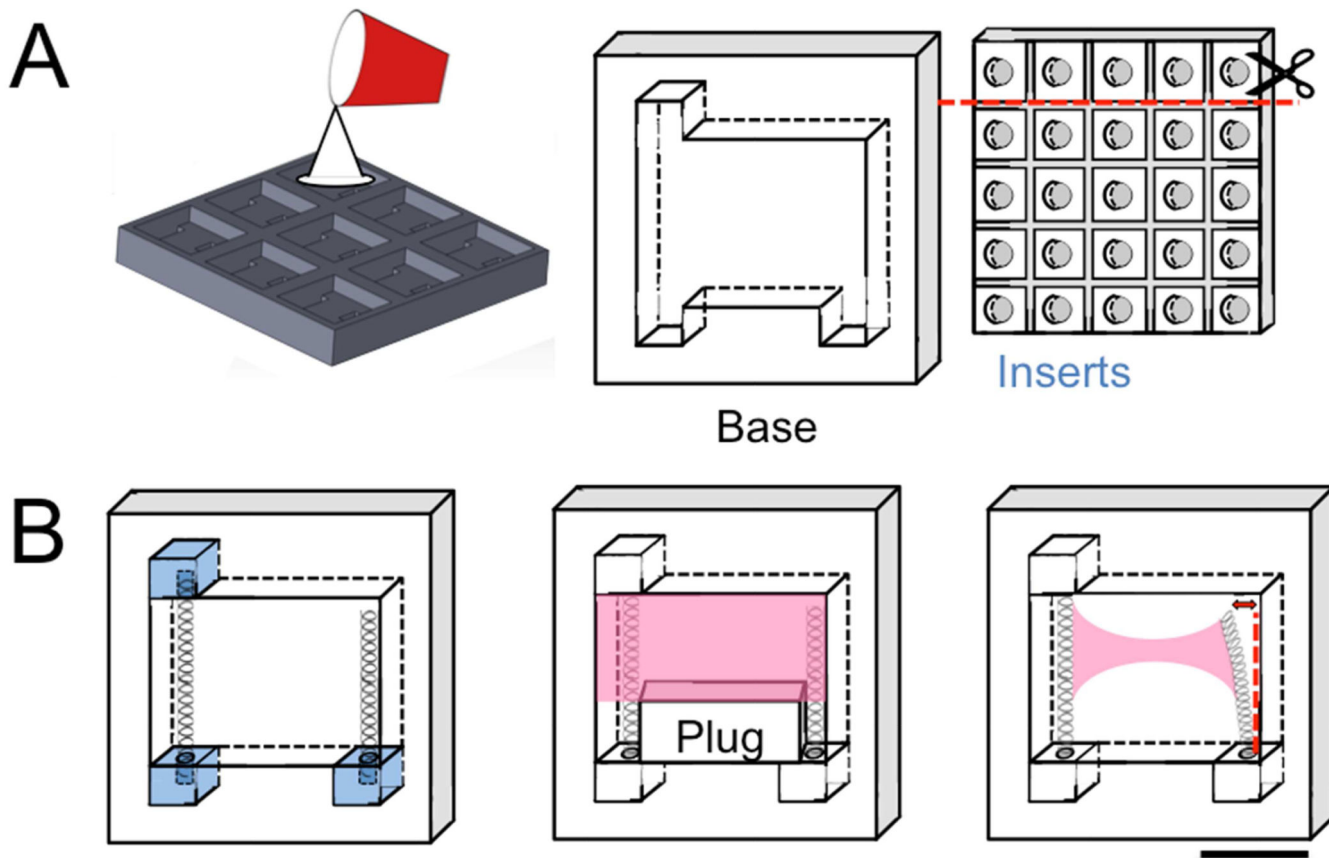


Fig. 1. Design and manufacturing of system

A. Custom molds machined from polycarbonate. B. Inserts and springs were inserted into device base to form complete system (left). Temporary plug prevented downward flow of collagen hydrogel (pink) as VIC gels were applied to upper region of device (center). The plug was removed once the gel polymerized. Over 14 days, hydrogel+VIC contracted, deflecting cantilevered spring (right) by a measurable amount. Scale bar is 1 cm.

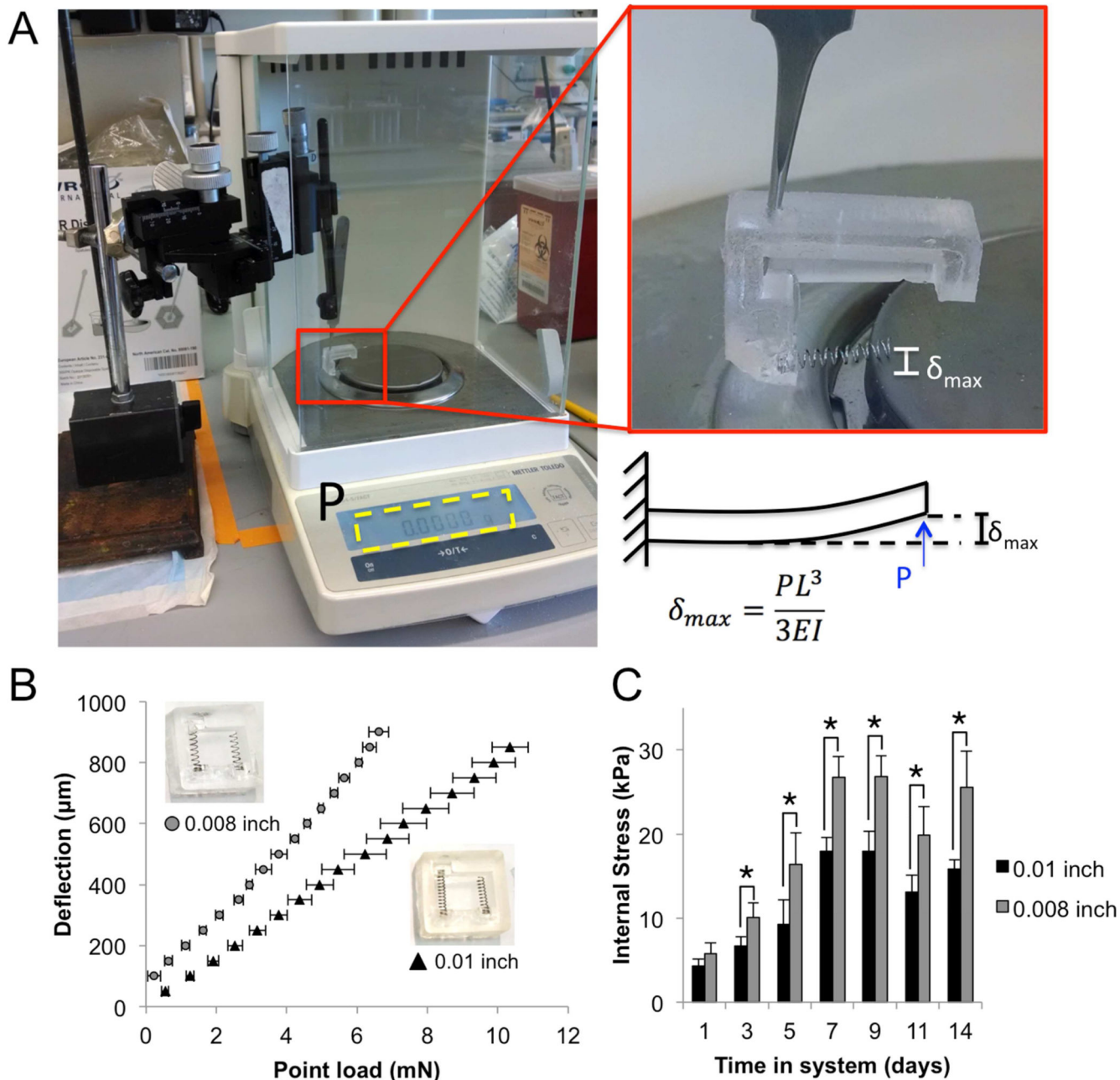


Fig. 2. Calibration of system to measure VIC contractility

A. Set-up for empirical calibration of spring in manufactured system. B. Deflection versus load curve for springs of two different wire thicknesses (0.01 and 0.008 inch). Inset photo shows systems with different thickness springs and corresponding symbol. C. Internal stresses developed in the hydrogels over 14 days of culture using springs with different wire thicknesses. Error bars are SEM. N=5 different systems tested for each type of spring.

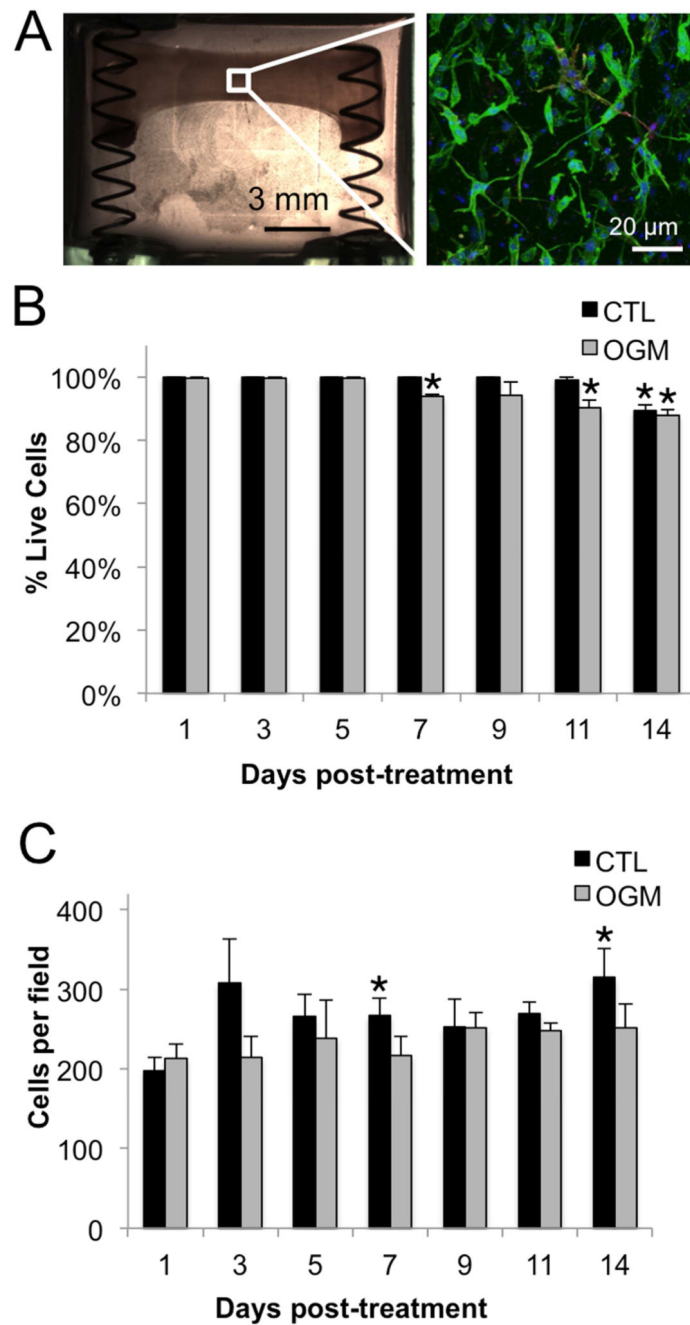


Fig. 3. Characterization of system to measure VIC contractility

A. Completed system at day 0, with hydrogel+VIC (left). F-actin (green), α SMA (red), and nuclei (blue) of hydrogel+VIC after 24 hours of culture in control media (right). B. Cell viability in control and osteogenic conditions over 14 days of culture in the system. C. Cell density in control and osteogenic conditions over 14 days of culture in the system. N = 3. * indicates $p < 0.05$ versus day 1 control. Error bars indicate SEM.

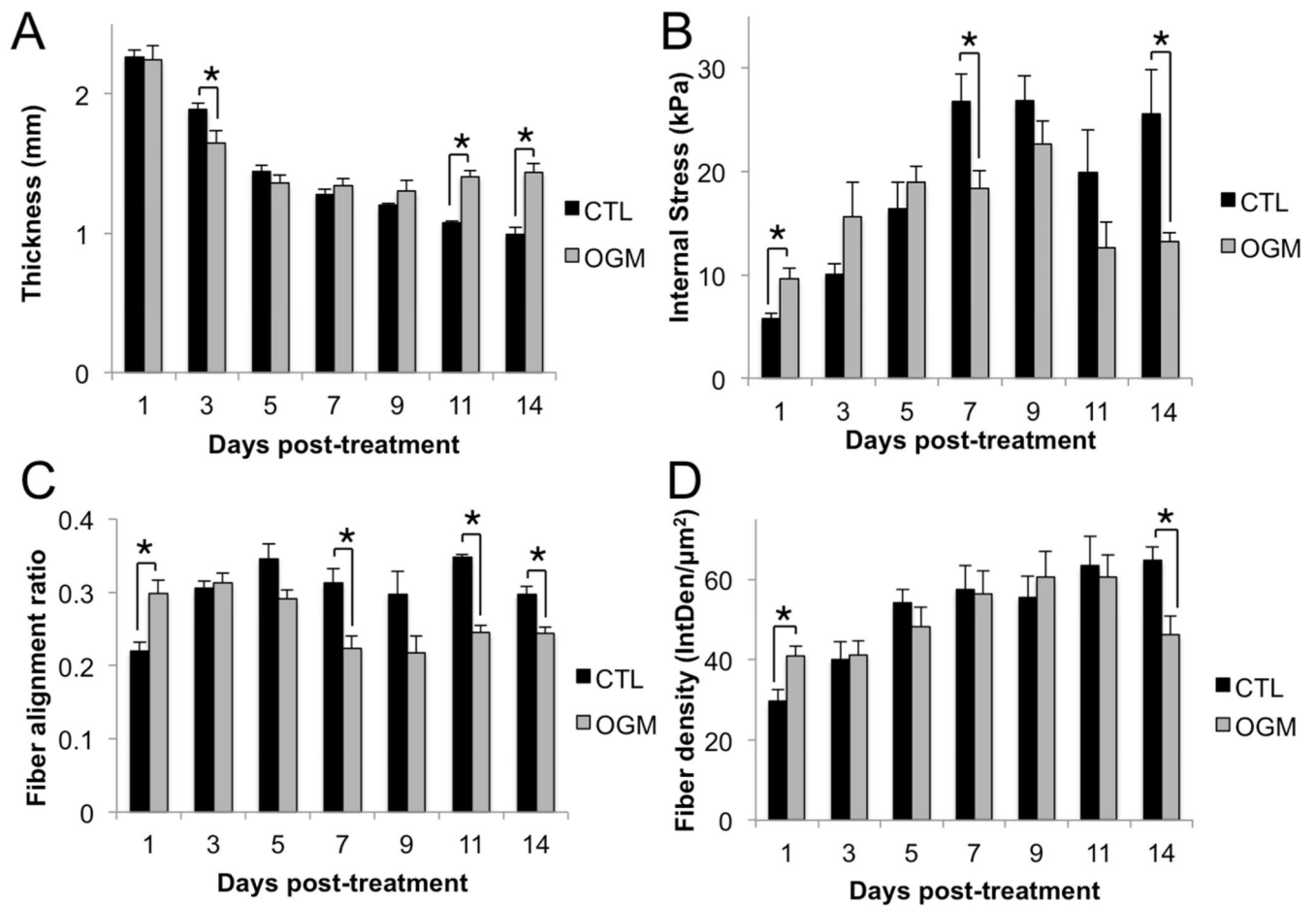


Fig. 4. Pro-osteogenic environment disrupts native mechanical activity of VIC

A. Thickness of the hydrogels. Thickness was measured every 48 hours over 14 days in control and osteogenic conditions. B. Internal stress in hydrogels. Stress was calculated from force exerted by VIC on the spring divided by the cross-sectional area of the gel at the thinnest point. C. Alignment of collagen fibers in the hydrogels. Alignment ratio of 1 indicates perfect alignment with direction of tension in hydrogel, alignment of 0 indicates fibers perpendicular to direction of tension. D. Density of collagen fibers in the hydrogels calculated from areal integrated density ($\text{IntDen}/\mu\text{m}^2$), the sum of the values of the pixels in the image divided by the area of the image. $N = 4$ for all experiments, * indicates $p < 0.05$ between groups indicated by bars, error bars indicate SEM.

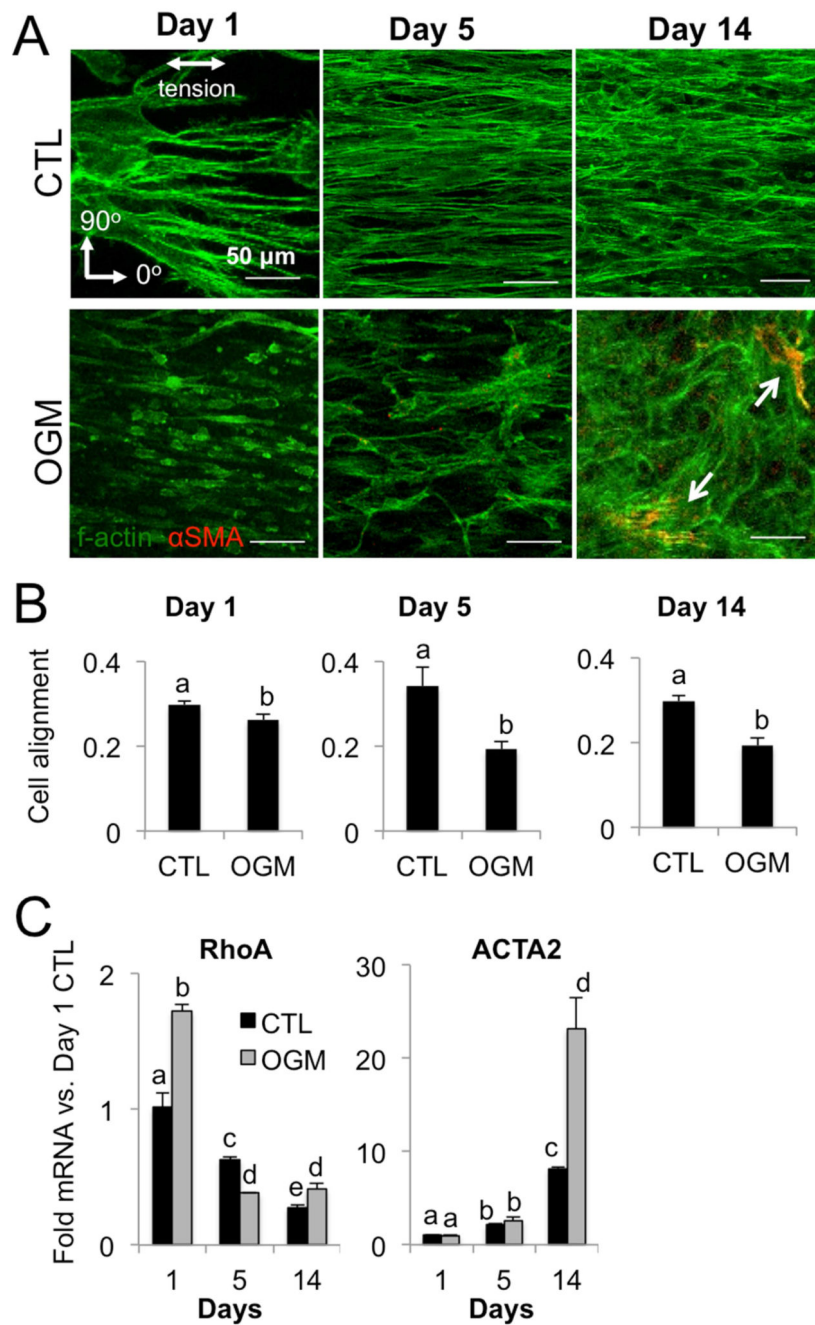


Fig. 5. Pro-osteogenic environment increases VIC myofibroblastic signaling

A. F-actin (green) and α SMA (red) in control or osteogenic condition at day 1, 5, and 14. Scale bar is 50 μ m. B. Alignment of VIC in control or osteogenic condition at day 1, 5, and 14, where a value of 1 indicates cells are perfectly aligned with the direction of tension. C. RhoA and ACTA2 mRNA in control or osteogenic condition at day 1, 5, and 14. N = 3 for all experiments. Bars with different letters are statistically different ($p < 0.05$), error bars indicate SEM.

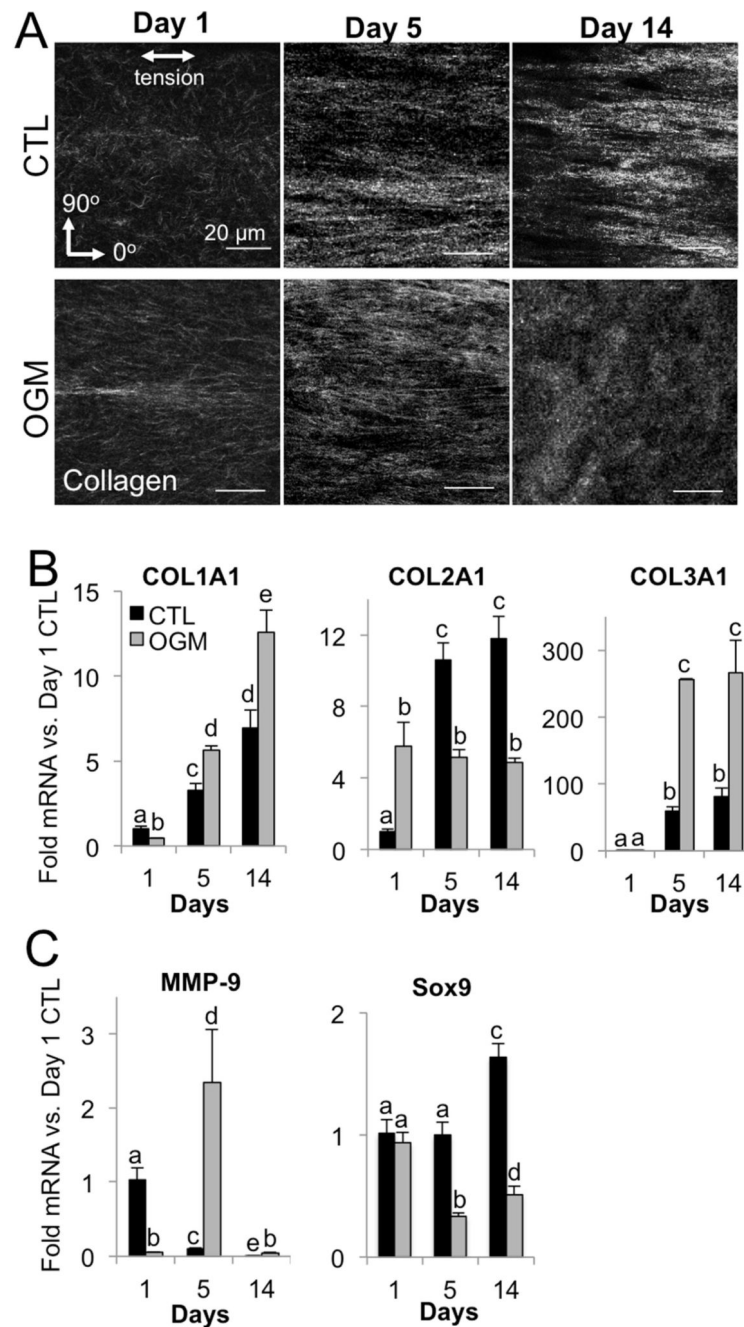


Fig. 6. Pro-osteogenic environment disrupts VIC organization of collagen matrix

A. Representative images of collagen fibers in control and osteogenic hydrogels at day 1, 5, and 14. B. Collagen isoform mRNA control and osteogenic hydrogels at day 1, 5, and 14. C. MMP-9 and Sox9 mRNA in control and osteogenic hydrogels at day 1, 5, and 14. $N = 3$ for all experiments. Bars with different letters are statistically different ($p < 0.05$), error bars indicate SEM.

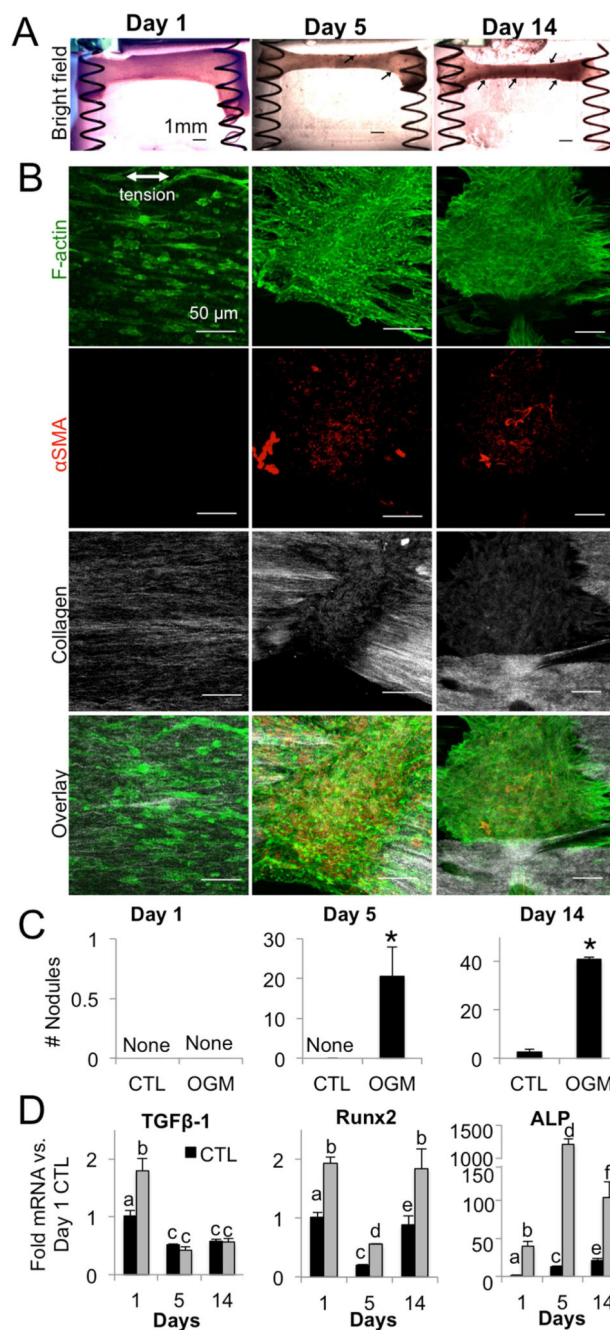


Fig. 7. Nodules and osteogenic signaling in mechanically active VIC hydrogels
 A. Bright-field images of osteogenic hydrogels at day 1, 5, and 14. Arrows indicate nodules.
 B. Immunofluorescence of osteogenic hydrogels at day 1, 5, and 14. Green = f-actin, red = α SMA, white = collagen.
 C. Number of nodules formed in control and osteogenic hydrogels at day 1, 5, and 14.
 D. TGF- β 1, Runx2, and ALP mRNA in control and osteogenic hydrogels at day 1, 5, and 14. N = 4 for all experiments. Bars with different letters are statistically different ($p < 0.05$), error bars indicate SEM.

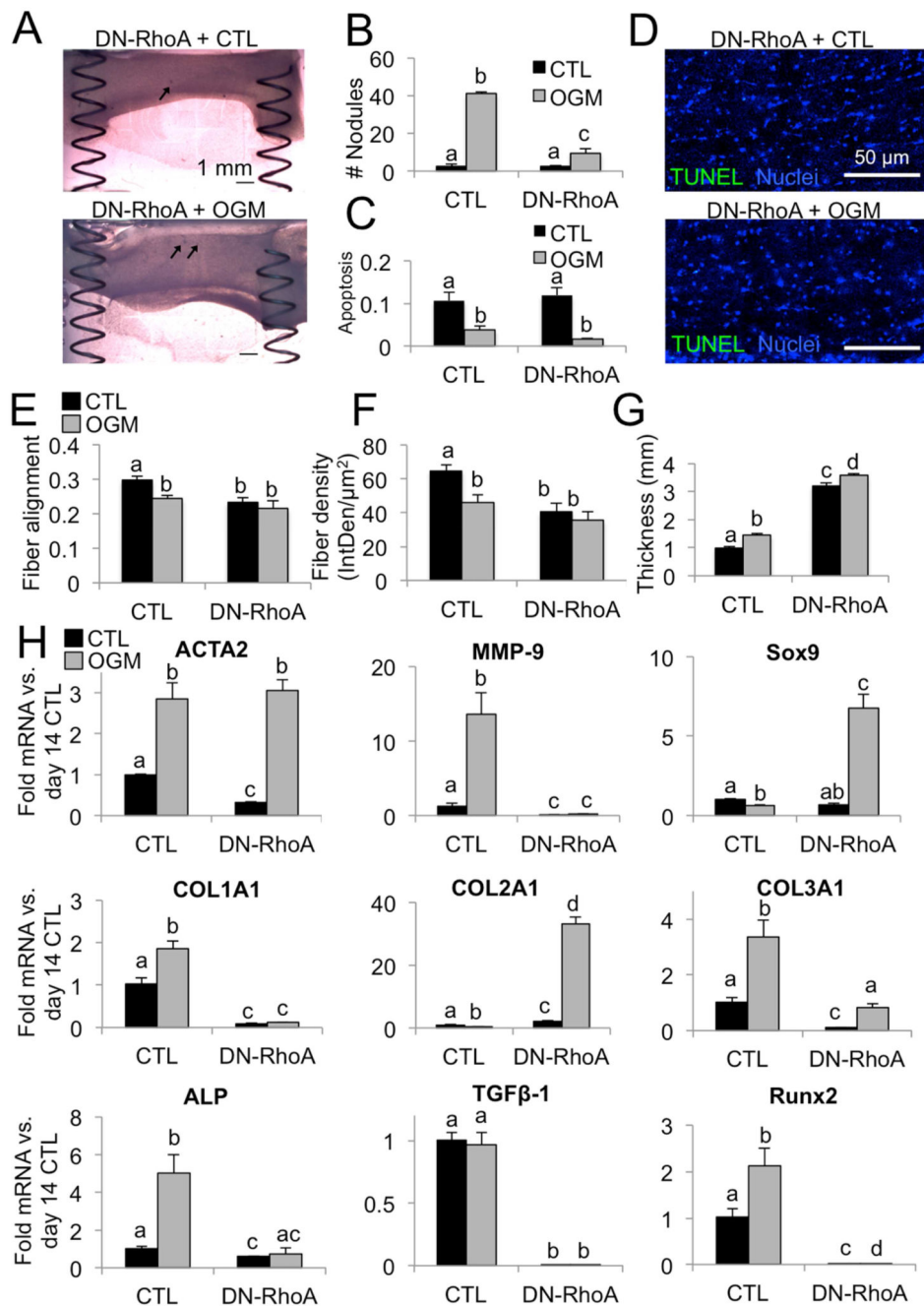


Fig. 8. Osteogenic and chondrogenic effects of RhoA inhibition

A. Brightfield images of VIC+DN-RhoA, control and osteogenic condition at day 14, showing reduction in nodule formation (arrows). Scale bar is 1mm. B. Number of nodules per gel at day 14. N = 4. C. Proportion of apoptotic cell nuclei in day 14 VIC+empty vector and +DN-RhoA, control or osteogenic treatments. D. Representative images of day 14 VIC +DN-RhoA gels control or osteogenic treatment. Scale bar is 500μm. E. Quantification of fiber alignment at day 14. A value of 1 indicates cells are perfectly aligned with the direction of tension. F. Quantification of fiber density. G. Quantification of gel thickness. H. Analysis

of mRNA for matrix remodeling, collagen isoforms, and pro-osteogenic genes in VIC+DN-RhoA, control or osteogenic condition at day 14. N = 3 for all experiments. Bars with different letters are statistically different ($p < 0.05$), error bars indicate SEM.

Author Manuscript

Author Manuscript

Author Manuscript

Author Manuscript

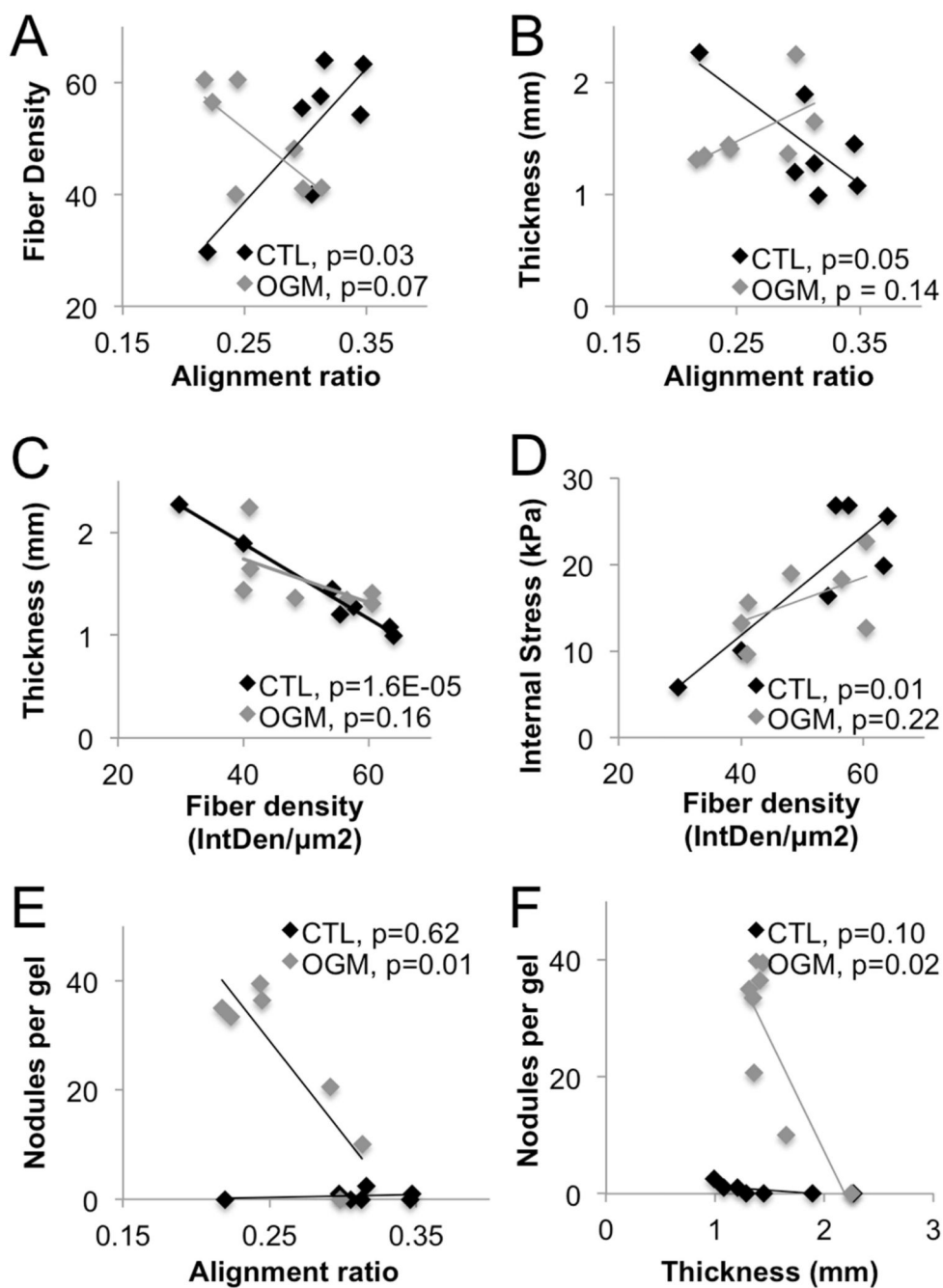


Fig. 9. Collagen fiber dynamics correlate with VIC mechanical activation

Analysis of Pearson's linear correlation coefficient between different sets of mechanical, biological, and pathological outputs in the VIC+hydrogel spring systems. All data sets include days 1 through 14. Only comparisons with at least one statistically significant correlation ($p < 0.05$) are shown, all other comparisons were not significant. OGM = osteogenic treatment.

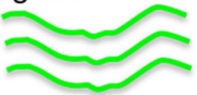
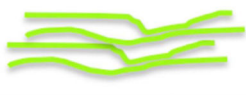

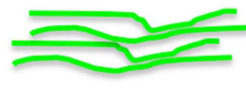















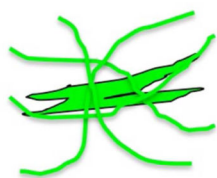
	Day	1	5	14
Collagen	CTL	Moderately dense, somewhat aligned 	More dense, somewhat aligned 	Most dense, very aligned 
	OGM	Moderately dense, aligned 	More dense, somewhat aligned 	Most dense, misaligned 
Cells Quiescent VIC:  Myofibroblastic VIC: 	CTL	Moderately dense, somewhat aligned 	More dense, aligned 	Most dense, very aligned 
	OGM	Moderately dense, somewhat aligned 	Moderately dense, misaligned 	Most dense, misaligned 
Calcification Osteoblast-like cell:  Myofibroblastic cell:  Calcium: 	CTL	No nodules	No nodules	Very few nodules
	OGM	No nodules	> 15 nodules 	> 35 nodules 

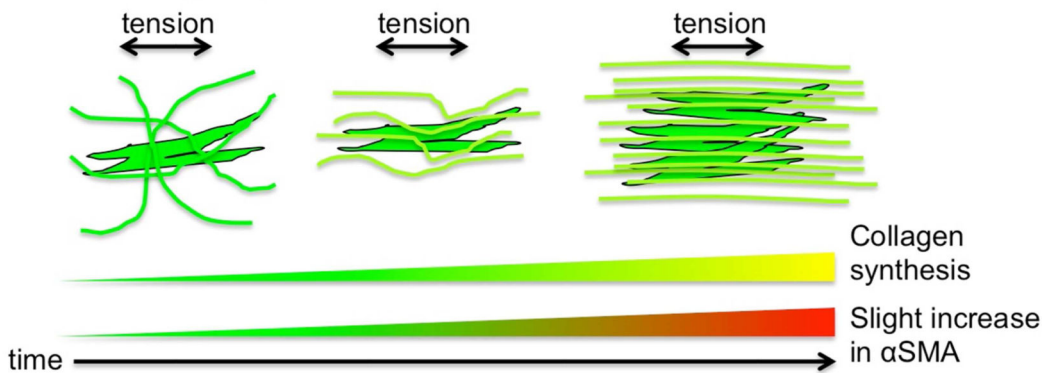
Fig. 10. Tri-phasic dynamics of collagen, cells, and calcification in VIC in tensioned hydrogels
Conceptual representation of the three phases of VIC time-dependent response to culture in the mechanically tensioned system under control or osteogenic conditions. Collagen response only differentiates in last phase (day 14), where cell and pro-calcific response begins at day 5.

VIC in non-tensioned hydrogel environment



Inactive RhoA
No α SMA

VIC in tensioned hydrogel environment



VIC in tensioned hydrogel environment + osteogenic stimulus

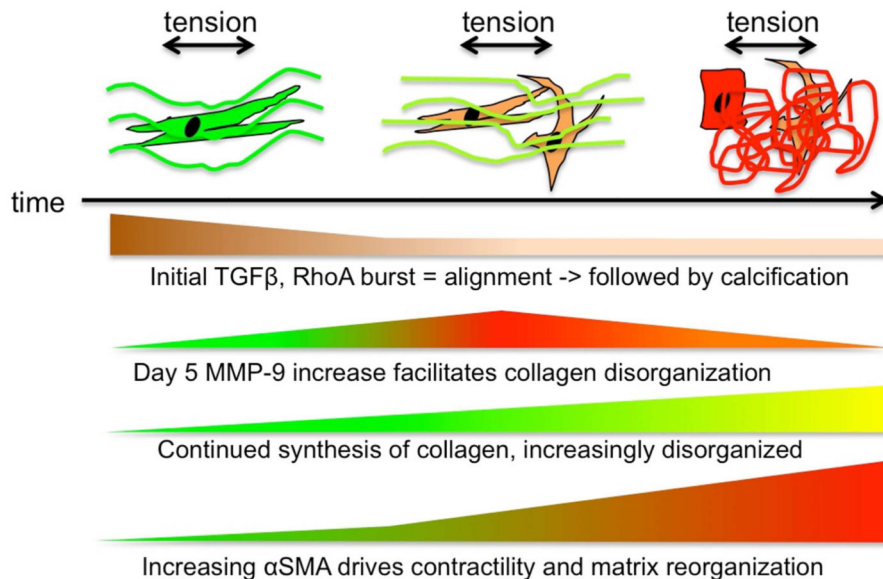


Fig. 11. Interactions between cells, collagen, signaling molecules, and tension

Conceptual representation of the different components of the system. In contrast to a non-tensioned culture environment, tension induces collagen synthesis and alignment. Osteogenic condition elicits complex time-dependent pathological response that results in reorganization of the extracellular matrix.

Table 1**Spring Parameters**

Spring Parameter	Spring 1	Spring 2
Wire diameter	0.008 in	0.01 in
Outside diameter	0.088 in	0.088 in
Hole diameter	0.094 in	0.094 in
Load at solid length	0.333 lb	0.666 lb
Rate	0.70 lb/in	1.10 lb/in
Part ID	CI 008B 09	CI 010B 13

Author Manuscript

Author Manuscript

Author Manuscript

Author Manuscript

Table 2
Quantitative rt-PCR primers

Gene	Forward	Reverse
18S	AATGGGGTTCAACGGGTTAC	TAGAGGGACAAGTGGCGTTC
RhoA	AACAGGATTGGTGCTTTTGG	CAGCAGGGTTTCACAAGACA
ACTA2	CAGCCAGGATGTGTGAAGAA	TCACCCCTGATGTCTAGGA
COL1A1	AGAAGACATCCCACCAGTCA	CGTCATCGCACACACATTG
COL2A1	GTCTACCCCAATCCAGCAA	GTCTACCCCAATCCAGCAA
COL3A1	TTGGCCCTGTTTGCTTTTAA	TGGTTGACAAGATGAGAACAAAA
MMP-9	ACACACACGACATCTTCC	AAGGTCACGTAGCCACAA
Sox9	GGGAGACTGCTGAATGAGAGC	CGTTCTTCACCGACTTTCTC
TGF-β1	CCACTCTCAGCCTCTCTGCT	TGGGTTCTCGGTATCCTACG
Runx2	GCACTACCCAGCCACCTTAA	TATGGAGTGCTGCTGGTCTG
ALP	ATGAGCTCAACCGGAACA	GTGCCCATGGTCAATCCT